Journal of Applied Electrochemistry **29**: 703–717, 1999.

Time-dependent polarization behaviour of pipeline grade steel in low ionic strength environments

S.L. CARSON and M.E. ORAZEM*
Department of Chemical Engineering, University of Florida, Gainesville, FL 32611-6005, USA
*(*author for correspondence, e-mail: meo@electro.che.ufl.edu)*

Received 12 December 1997; accepted in revised form 18 August 1998

Key words: calcareous deposits, cathodic protection, polarization

Abstract

A bench-top experimental approach is described for estimation of the polarization behaviour of pipeline steel as a function of the time-dependent formation of scale and calcareous deposits in simulated soil leachates. A three-time constant process model provided a common set of parameters for a given soil environment and level of aeration. The parameters estimated could be applied to a broad range of current values and were independent of time, potential and applied current. The experimental approach, model and regression procedure are general and could be used to determine the physical parameters associated with the seasonal variations (wet–dry cycles) in the soils surrounding pipelines or with other factors that influence general corrosion. The polarization model could provide a boundary condition for mathematical models for cathodic protection of pipelines or other buried structures. The separation of current contributions implicit in the model can be used to assess the reduction of corrosion current associated with specific CP criteria.

List of symbols

a_0	constant in the time-domain measurement model, Equation 17 (V)
a_m	constant in the time-domain measurement model, Equation 17 (V)
b_n	constant in the time-domain measurement model, Equation 17 (V)
E	potential, Equation 10 (V)
$E_{\text{comp},k}$	calculated *IR* compensated potential, Equation 3 (V)
$E_{\text{IR},k}$	measured off-potential, Equation 1 (V)
$E_{\text{meas},k}$	measured on-potential, Equation 3 (V)
$E_{\text{pred},k}$	predicted on-potential, Equation 1 (V)
E^*_{Fe}	reference potential for corrosion reaction, Equation 13 (V)
$E^*_{\text{H}_2}$	reference potential for hydrogen evolution reaction, Equation 10 (V)
ΔE_k	Ohmic drop at time t_k, Equation 2 (V)
F	objective function, Equation 15, mA m^{-2}
f_{Fe}	exponential decay function, Equation 11 (dimensionless)
$f_{\infty,\text{Fe}}$	final reaction current fraction, Equation 12 (dimensionless)
f_{H_2}	exponential decay function, Equation 8 (dimensionless)
f_{∞,H_2}	final reaction current fraction, Equation 9 (dimensionless)
f_{O_2}	exponential decay function, Equation 6 (dimensionless)
f_{∞,O_2}	final reaction current fraction, Equation 7 (dimensionless)
$I_{\text{appl},k}$	applied current, Equation 2 (mA)
i_{Fe}	iron oxidation current density, Equation 5 (mA m^{-2})
i^*_{Fe}	initial current density, Equation 11 (mA m^{-2})
i_{H_2}	hydrogen evolution current density, Equation 5 (mA m^{-2})
$i^*_{\text{H}_2}$	initial current density, Equation 8 (mA m^{-2})
$\underline{i}k$	applied current density at time t_k, Equation 15 (mA m^{-2})
$\hat{\underline{i}}k$	model current density at time t_k, Equation 15 (mA m^{-2})
i_{O_2}	oxygen reduction current density, Equation 5 (mA m^{-2})
$i^*_{\text{O}_2}$	mass transfer-limited oxygen reduction current, Equation 6 (mA m^{-2})
i_{total}	net current density, Equation 5 (mA m^{-2})

$R_{cell,k}$ cell resistance at time t_k, Equation 2 (Ω)
$R_{cell,lm}$ time-varying cell resistance, Equation 4 (Ω)
$R_{cell,mean}$ constant cell resistance, Equation 3 (Ω)
t_k time point, Equation 16 (s)
V_{meas} measured potential, Equation 16 (V)
V_{mod} model value of the potential, Equation 16 (V)

Greek symbols

β_{Fe} Tafel slope for iron oxidation, Equation 13 (V (decade)$^{-1}$)
β_{H_2} Tafel slope for hydrogen evolution, Equation 10 (V (decade)$^{-1}$)
ε_k residual error, Equation 16 (V)
Φ_{ref} reference electrode potential, Equation 17 (V)
τ_{Fe} time constant for iron oxidation, Equation 12 (days)
τ_{H_2} time constant for hydrogen evolution, Equation 9 (days)
τ_m measurement model time constant, Equation 17 (days)
τ_n measurement model time constant, Equation 17 (days)
τ_{O_2} time constant for oxygen reduction, Equation 7 (days)

1. Introduction

This work was motivated by the need to determine the electrochemical properties of steel as a function of time for two related applications. The first application was to find a method to establish suitable criteria for cathodic protection. Presently, several criteria are used to indicate that satisfactory levels of cathodic protection have been achieved [1–3]. In one criterion, cathodic protection is assumed to have been achieved if the applied current shifts the steel potential a set amount (e.g., −100 mV) from the depolarized corrosion potential. In another, an IR-corrected potential reading of –850 mV ($Cu/CuSO_4$) is assumed to indicate that satisfactory protection has been achieved. It can be expected that the environment of the pipe will influence the corrosion current seen at any given applied potential; thus, a method is needed to determine whether the corrosion current is reduced sufficiently when such criteria are applied. The second application was to provide a method to establish parameters for polarization curves that can be used in mathematical models for cathodic protection which account for the electrochemistry at steel surfaces (e.g., [4–13]).

At cathodic potentials, calcareous and rust scales can form due to localized alkalinity associated with oxygen reduction or hydrogen evolution at the steel surface [14]. The similar values for the time constants associated with mass transfer transients and those associated with changes in scale thickness or resistance complicates measurement of polarization parameters for steel in soil and seawater environments [15]. A dynamic potential or current scan must be conducted slowly enough to avoid artifacts associated with transient accumulation or depletion of ionic species in the diffusion layer and fast enough that the changes in current and potential do not disrupt or alter the calcareous and scale deposits. In practice, there is no suitable scan rate that can be applied to obtain artifact-free potentiodynamic or galvanodynamic polarization curves [15].

In this paper, a method is described which provides an estimate for time-dependent polarization curves. The experimental approach followed that of Nisancioglu et al. [4, 15] in which a polarization curve is constructed from a family of galvanostatic experiments conducted for a given environment. The mathematical formulation of the polarization curve represents an extension to that described by Nisancioglu et al. [4–6, 15], and model parameters were obtained by regression to the family of galvanostatic potential–time traces. Once the model parameters were estimated, effective current–potential curves could be calculated for any desired time. The design of the model allowed the determination of the contributions of the individual reactions to the total current at any desired time and therefore could be used to establish the effect of meeting a specific CP criterion. The time-dependent polarization behaviour of steel can be obtained for different aqueous environments. The focus of the present work was on low ionic-strength, high-moisture content sand-filled environments which are intended to simulate real soil environments [16].

2. Background

At potentials cathodic to the corrosion potential of steel, reduction of water and of dissolved oxygen causes the pH near the steel surface to be higher than that in the surrounding soil [14, 17]. The high cation concentration at the steel surface needed to satisfy electroneutrality facilitates precipitation reactions [14, 17]. Precipitation of calcium carbonate and magnesium carbonate can occur in the presence of carbonate or bicarbonate ions.

The source of carbonate ions in natural waters can be a mineral leachate or a product of dissolved carbon dioxide associated with aeration [17]. Magnesium hydroxide, which can precipitate at pH values higher than 9.5, is also observed in calcareous films [17, 18]. Calcareous deposits formed in sea water have been found to contain sodium, iron, silicon and strontium [14]. In natural groundwaters, the cation content is a function of the mineral content of the surrounding soil [16].

Calcareous deposits reduce corrosion rates by providing a barrier to mass transfer of oxygen or by inhibiting the hydrogen evolution reaction [4–6, 15]. In this paper, the corrosion reaction is treated as being inhibited by calcareous deposition. Deslouis et al. [20] report that the calcareous deposits formed under cathodic protection in waters containing both Ca^{2+} and Mg^{2+} consist of calcite and argonite crystals and has both a partial blocking and a porous behaviour. The formation of calcareous deposits reduces the amount of current required to achieve a given level of cathodic polarization and, therefore reduces the current requirements for cathodic protection [15]. The effects of calcareous deposition on the potential–current behaviour of a steel surface have been studied for synthetic and natural sea waters [4–6, 15], but a similar mechanistic study has not been done for the influence of calcareous deposits in soil leachates which have a much lower ionic content.

3. Experimental method

The experimental approach followed that of Nisancioglu et al. [4, 15] in which polarization parameters are constructed from a family of galvanostatic experiments conducted for a given environment. Application of constant current was chosen because, in potentiostatic experiments, both the current and the surface overpotential change in response to changes in the ohmic potential drop.

3.1. *Cell design*

Cylindrical coupons, approximately three inches in length and one-half inch in diameter, were milled out of API5LX52 pipeline steel. The coupons were ultrasonically cleaned in ethanol and in distilled water before use, but other metallurgical pretreatment such as polishing or annealing was not used. Platinum served as the counter electrode to the 5LX52 steel.

The cell (Figure 1) consisted of the API5LX52 cylindrical working electrode placed at the centre of a 5.41 cm (2.13 in) radius Nalgene jar with four 0.635 cm (0.25 in) strips of platinum (0.025 mm thick) placed 90° apart at a distance of 4.75 cm (1.87 in) from the centre of the cell [21]. The symmetric placement of more than one counter electrode around a working electrode increased the uniformity of current distribution with respect to use of a single counter electrode [22]. A calomel reference electrode was placed between two counter electrodes (45° from either anode) at a distance 4.1 cm (1.6 in) from the centre of the cell. The bottom circular surface of the steel electrode was masked by a thin epoxy (Hexcel Epolite 2410) disc. Both working and counter electrodes had a perpendicular contact with the bottom of the cell. This design provided a uniform distribution of current without completely encircling the working electrode with platinum. The current distribution for the working electrode surrounded by four anodes was calculated using the boundary element model described in [12] to be uniform to within better than 0.1% of the mean applied current density.

Electrolyte replenishment was needed to avoid transients associated with changes in electrolyte composition. Electrolyte was dripped down a tube installed normal to the bottom of the cell, located approximately 0.635 cm (0.25 in) from the center of the cell between two anodes (45° from each) and 90° from the reference electrode. This design avoided formation of ground loops between cells. An outlet tube was placed on the side of the cell approximately 3 cm (1.2 in) from the bottom. The electrolyte level did not extend above the level of this outlet.

Eight cells of this design were immersed in a temperature-controlled water bath maintained at a temperature of $20 \pm 2\,^{\circ}C$. Electrolyte was prepared in 50 L of deionized water. The oxygen content of the electrolyte was controlled by sparging either industrial grade Argon or air scrubbed of CO_2 by passing it through Ascarite II. The sparging process was begun 24 h prior to the addition of ionic species. The oxygen content after deaeration ranged from 1.5 to 3.5 ppm, and the oxygen content after aeration ranged from 7.5 to 8.5 ppm. Aeration or deaeration was maintained throughout the experiment. Aeration of electrolyte droplets by contact with air was minimized by maintaining a hydrated Argon atmosphere inside the tube. The hydrated gas produced from the reservoir bubbler was released into the atmosphere for the aerated electrolyte experiments and into the drip tubes for the deaerated electrolyte experiments. The electrolyte feed tube was split into eight lines and electrolyte was fed into each cell. The flow rate was monitored using glasstube Teflon-bead flowmeters. All experiments were performed in an inert solid matrix (silicate sand) to inhibit any convection in the cells.

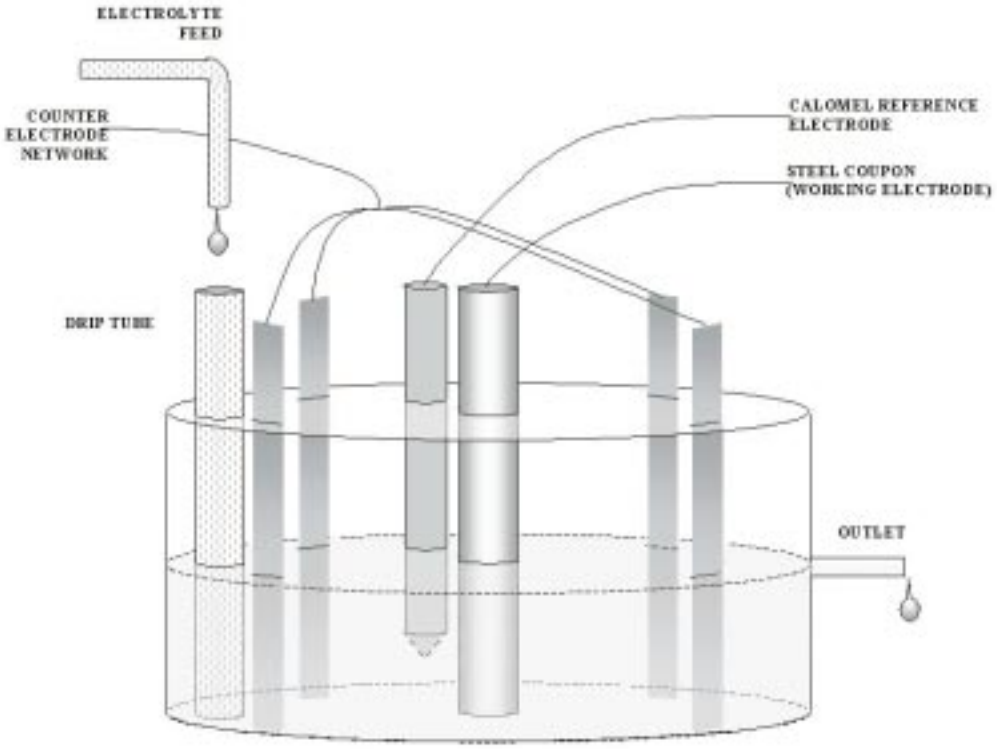

Fig. 1. Design of experimental cell. Steel working electrode located in centre of cell is surrounded by a network of platinum counter electrodes. SCE between two platinum electrodes is for sensing. Electrolyte is constantly replenished by dripping feed into cell. Liquid level of cell is maintained by electrolyte dripping from outlet.

3.2. *Data acquisition*

A Gamry Instruments PC3 potentiostat/galvanostat/ZRA Board was installed in a personal computer and connected to a Gamry Instruments ECM8 electrochemical multiplexer. The multiplexer allowed eight cells to be simultaneously and independently controlled. The Gamry hardware was controlled using the Gamry CMS100 and CMS208 software packages.

Hardware and code were developed to convert the ECM8 potentiostat into a galvanostat. The CMS208 galvanic corrosion routine was altered and used to apply a constant potential across a 1000 Ω resistor. A constant current was thereby applied between the working and counter electrode by connecting the working electrode to the resistor and connecting the counter and reference electrodes to the ECM8.

A filtering procedure was used to reduce stochastic noise in the potential and current measurements. Twenty points were collected over 2.0 s. Current–time values and potential–time values were then fit to a line using least squares regression. The value of the line at the last sample time was stored as the value for that sample. To reduce the effect of switching multiplexer channels when a cell was sampled, the multiplexer was switched to the channel of a cell for one second prior to sampling.

Determination of the ohmic drop in each cell during the experiment was required for analysis of the data. Continuous *IR* compensation by current interruption was found to be unreliable; thus, the current was interrupted periodically for a small number of measurements. The CMS208 galvanic corrosion code was modified such that the on-potential of the steel electrode was measured for 100 points after which five off-potentials were measured using a current interrupt technique. This cycle was repeated throughout the experiment.

3.3. *Data conversion*

Current values were measured as the total current applied through the cell. Upon the completion of an experiment, each electrode was removed and the active surface height (exposed depth of the electrode in the

electrolyte) was measured, from which the active surface area was calculated.

The cell resistance was calculated using the ohmic drop determined from the on-potential and off-potential measurements. A line was fit to the five points collected just before and the five points collected just after the set of five current interrupt measurements using a least squares algorithm. The resulting line was used to predict the values of potential measurement including ohmic drop, $E_{\text{pred},k}$, at the time, t_k, of sampling of the current-interrupt point. The difference was calculated between the predicted potential including ohmic drop and the *IR* compensated measured potential, $E_{\text{IR},k}$:

$$\Delta E_k = E_{\text{IR},k} - E_{\text{pred},k} \tag{1}$$

The difference was then divided by the current applied, $I_{\text{appl},k}$, at that sampling time resulting in a value for the cell resistance

$$R_{\text{cell},k} = \frac{\Delta E_k}{I_{\text{appl},k}} \tag{2}$$

IR compensation was obtained using either the mean value of $R_{\text{cell},k}$ for the entire experiment, that is,

$$E_{\text{comp},k} = E_{\text{meas},k} + (I_{\text{appl},k} R_{\text{cell,mean}}) \tag{3}$$

or, for cases where the cell resistance was a function of time, using a cell resistance calculated for each set of five current interrupt measurements

$$R_{\text{cell,lm}} = \frac{\sum_{k=1}^{5} R_{\text{cell},k}}{5} \tag{4}$$

The previous 100 potential measurements were corrected for ohmic drop using this mean value.

3.4. *Electrolyte*

Two of the three electrolyte types employed in these experiments were selected to be consistent with previously analysed soil types [16]. One soil was relatively rich in both Ca^{2+} and Mg^{2+} and is labelled here as electrolyte HCHM. The other soil was relatively rich in Ca^{2+} but not in Mg^{2+} and is labeled here as electrolyte HCLM. Electrolyte HCLM has a lower ionic strength than electrolyte HCHM. The concentrations of the ionic species in each electrolyte type are given in [16] and Table 1.

The soil leachates were reproduced by dissolving appropriate amounts of reagent grade $Ca(OH)_2$, $CaCl_2$, K_2SO_4, $MgSO_4$, Na_2SO_4, and $NaHCO_3$ in 50 L of deionized water. As the leachate concentrations listed in reference [16] were not stoichiometrically balanced. $Ca(OH)_2$ and H_2SO_4 were added in to reach the necessary concentrations of calcium and sulfate. The HCHM electrolyte required SO_4^{2-} concentrations far greater than could be added using the solid species; thus, excess H_2SO_4 was added to reach the desired value. The solutions were titrated with NaOH and H_2SO_4 solutions to reach the desired pH. Thus, the ionic strengths of the simulated leachates were greater than the reported values, but the concentrations of the species involved with deposition of calcareous deposits were consistent with reported values. Only the Na^+ and SO_4^{2-}concentrations were higher than reported by Han [16].

Table 1. Concentrations of electrolytes simulating soil types described by Han [16]

Species	HCLM electrolyte		HCHM electrolyte	
	/mol	/ppm	/mol	/ppm
Na^+	0.001 28	23	0.003 00	275
K^+	0.000 611	11	0.000 278	5
Ca^{2+}	0.005 38	97	0.004 22	81
Mg^{2+}	0.000 33	6	0.002 05	37
HCO_3^-	6.67×10^{-5}	4 mg dm^{-3}	5.95×10^{-5}	5 mg dm^{-3}
SO_4^{2-}	0.001 24	78	0.003 66	480
Cl^-	0.002 55	46	0.003 07	65
Conductivity, /m Ω^{-1} cm^{-1}	0.8	–	1.9	–
Ionic strength	0.0162	–	0.0231	–

4. Polarization model

The mathematical approach taken in the present work follows the model developed by Nisancioglu et al. [4–6, 15] to describe the time-dependent polarization relationship associated with formation of calcareous deposits with the exception that an additional relaxation process needed to be introduced in order to obtain a model of general applicability. Parameters were obtained by regressing the resulting model to all potential–time traces obtained for a given environment.

4.1. *Physico-chemical model*

The total current to the surface

$$i_{\text{total}} = i_{O_2} + i_{H_2} - i_{\text{Fe}} \tag{5}$$

was assumed to consist of contributions from corrosion i_{Fe}, oxygen reduction i_{O_2}, and hydrogen evolution i_{H_2}. The oxygen reduction reaction was assumed to be mass

transfer-limited, and the growth of calcareous deposits was assumed to reduce the value of the mass transfer-limited current by a factor f_{O_2} such that

$$i_{O_2} = i^*_{O_2} f_{O_2} \tag{6}$$

where f_{O_2} was assumed to have an exponential decay from an initial value of one to a long-time value f_{∞,O_2} as

$$\frac{f_{O_2} - f_{\infty,O_2}}{1 - f_{\infty,O_2}} = \exp(-t/\tau_{O_2}) \tag{7}$$

The growth of calcareous deposits was assumed to reduce the value of the hydrogen evolution current by a factor f_{H_2} such that

$$i_{H_2} = i^*_{H_2} f_{H_2} \tag{8}$$

where

$$\frac{f_{H_2} - f_{\infty,H_2}}{1 - f_{\infty,H_2}} = \exp(-t/\tau_{H_2}) \tag{9}$$

The hydrogen reaction was assumed to be kinetically controlled, that is,

$$i^*_{H_2} = 10^{(E - E^*_{H_2})\beta_{H_2}} \tag{10}$$

As Equation 10 shows no dependence on mass transfer, the manner in which calcareous films were assumed to reduce the rate of hydrogen evolution is different than that envisioned for oxygen reduction. The film may act to poison the reaction or act as a barrier to the formed hydrogen gas molecules.

In contrast to the model presented by Nisancioglu et al. [4–6, 15], the calcareous deposits were assumed to reduce the current associated with corrosion. Thus,

$$i_{Fe} = i^*_{Fe} f_{Fe} \tag{11}$$

where

$$\frac{f_{Fe} - f_{\infty,Fe}}{1 - f_{\infty,Fe}} = \exp(-t/\tau_{Fe}) \tag{12}$$

and

$$i^*_{Fe} = 10^{(E - E^*_{Fe})/\beta_{Fe}} \tag{13}$$

This extension of the model of Nisancioglu et al. [4–6, 15] was motivated by results of a time-dependent measurement model analysis of several potential traces which indicated that three exponential decay time constants were resolvable from the data (see Appendix); whereas, the model of Nisancioglu et al. [4–6, 15] included only two time–dependent processes.

The current can be expressed in terms of all polarization parameters as

$$\begin{aligned} i = {} & i^*_{O_2} f_{\infty,O_2}[1 - \exp(-t/\tau_{O_2})] + i^*_{O_2} \exp(-t/\tau_{O_2}) \\ & + 10^{(E - E^*_{H_2})/\beta_{H_2}} f_{\infty,H_2}[1 - \exp(-t/\tau_{H_2})] \\ & + 10^{(E - E^*_{H_2})/\beta_{H_2}} \exp(-t/\tau_{H_2}) \\ & - 10^{(E - E^*_{Fe})/\beta_{Fe}} f_{\infty,Fe}[1 - \exp(-t/\tau_{Fe})] \\ & - 10^{(E - E^*_{Fe})/\beta_{Fe}} \exp(-t/\tau_{Fe}) \end{aligned} \tag{14}$$

The calcareous deposits were assumed to influence only the preexponential terms in Equations 8 and 11 through the factors f_{H_2} and f_{Fe}, respectively. The Tafel slope parameters and effective equilibrium potentials (Equations 10 and 13) were therefore assumed to be independent of both potential and time.

4.2. *Regression procedure*

In addition to the use of an extra time constant to account for growth of calcareous deposits, the present work is distinguished from the previous approach by the manner in which model parameters were obtained. Nisancioglu et al. [4–6, 15] employed a stepwise procedure for parameter estimation. The mass transfer-limited oxygen reduction current was obtained either through extrapolation of potentiodynamic scans or through use of mass transfer correlations. The Tafel slopes were assumed to have values corresponding to bare steel. The time constant for hydrogen evolution was assumed to have an infinitely large value; thus the time dependence on hydrogen evolution was effectively removed from the model. The reduced set of unknown parameters was obtained by regression. Noninfinite values for τ_{O_2}, the time constant associated with the exponential decay of the oxygen reduction current, were only found for total currents which were greater than 0.5 $i^*_{O_2}$. The resulting parameter space was therefore valid only for cathodic currents larger than 0.5 $i^*_{O_2}$, and the model parameters such as τ_{O_2} were found to be functions of current density.

Within the present work, Equation 14 was regressed to a data set for each electrolytic environment (consisting of data from up to eight individual cells). An unweighted nonlinear least-squares technique was employed where the objective function

$$F = \sum_{k=1}^{n} \left(\underline{i}_k - \hat{\underline{i}}_k\right)^2 \tag{15}$$

was minimized and where $\underline{i}_k$ is the applied current density at time t_k and $\underline{i}_k$ is the value of the current given by Equation 14. The Levenberg–Marquardt method [23] was used to obtain the set of eleven parameters in the model which minimized the value of Equation 15.

5. Results and discussion

The physico-chemical model was regressed to galvanostatic data. Time-dependent current–potential curves could be synthesized for the environments for which the model was employed. The estimated parameter sets for each environment demonstrated consistency with prior findings.

5.1. *Regression*

The current values applied to each of eight cells were selected to encompass potentials both anodic and cathodic to the open-circuit condition. The three potential–time traces for the aerated HCHM electrolyte shown in Figure 2 represent an anodic, a cathodic, and the open circuit condition. The potential values have been corrected for ohmic drop. The mean resistance of each cell was $(157 \pm 8)\,\Omega$. The bimodal character of the potential traces was shown to be consistent with minor fluctuations of the electrolyte level in the cell.

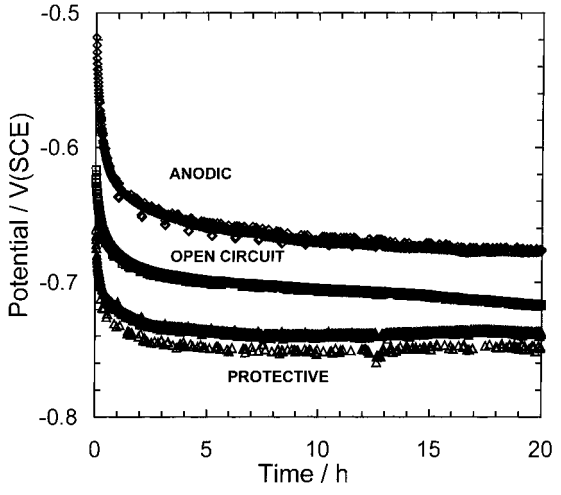

Fig. 2. Three representative potential–time traces at three applied currents: anodic $0.808\,\mathrm{A\,m^{-2}}$ ($75.1\,\mathrm{mA\,ft^{-2}}$); cathodic $-0.251\,\mathrm{A\,m^{-2}}$ ($-23.3\,\mathrm{mA\,ft^{-2}}$); and zero net current.

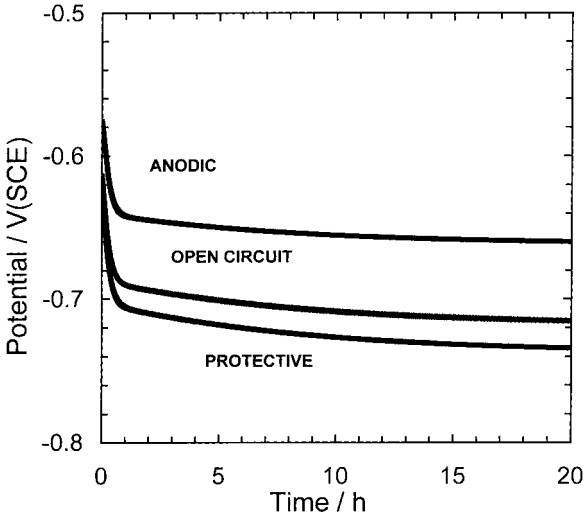

Fig. 3. Model values corresponding to three potential–time traces shown in Figure 2.

The model values corresponding to the three traces shown in Figure 2 are presented in Figure 3. The residual error for the regression is given by

$$\varepsilon_k = V_{\mathrm{meas}}(t_k) - V_{\mathrm{mod}}(t_k) \tag{16}$$

where V_{meas} and V_{mod} are the measured and model values, respectively, for potential at time t_k. The residual errors for the regression are presented in Figure 4. Even for the most cathodic current, which has the least adequate fit, the residual errors were very small. The residual errors were of the order of 10 mV for the anodic and cathodic curves and 2 mV for the open-circuit curve.

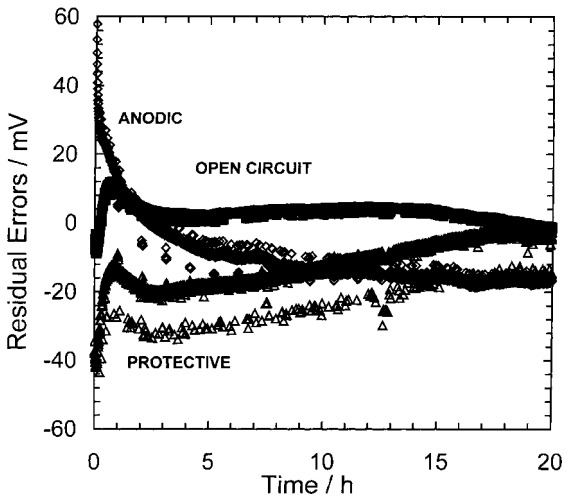

Fig. 4. Residual errors between model values in Figure 3 and measured potential–time traces in Figure 2.

The larger errors at short times may be associated in part with uncertainty concerning the start-up time and initial surface condition.

Potential data collected at extremely cathodic currents was often not used in these regressions. In some cases, the data showed discontinuous behaviour that was associated with nucleation, growth, and detachment of hydrogen bubbles. Bubble formation can affect the potential at the surface by blocking the electrode surface (decreasing current density), by blowing off calcareous film (increasing current density), and by introducing hydrodynamics near the surface that are different than the hydrodynamics exhibited in the other cells under study. Use of a common set of parameters for each environment over the potential range studied requires that convection be independent of the applied current.

5.2. *Synthesized polarization curves*

The model parameters obtained by regression are presented in Table 2 for the environments evaluated in this study. The confidence intervals reported for these parameters are those determined by the regression. The parameters can be used to reconstruct a family of current–potential curves predicted using the model for specified times. The resulting set of current-potential curves for the aerated HCHM electrolyte is presented in Figure 5 for 0, 2, 5, 10, 30 and 50 h, and 10 days. The corresponding set of curves for the deaerated HCHM electrolyte is presented in Figure 6. The solid curve in Figures 5 and 6 that shows the most negative open circuit potential is the predicted curve at 10 days. The other solid curve is the predicted initial curve. The refined model and regression technique allowed the model to predict the potential-time behaviour over a wider range of currents than was possible using the previous result of Nisancioglu et al. [4–6, 15] The open circuit potential decreased with time and reached a steady state very rapidly, within two days, of approximately −710 mV vs SCE. The potential induced by a cathodic current decreased significantly over two days. A highly anodic current was predicted to produce an increasing anodic potential with time. This result was the least reliable in that only one anodic current value was used for the regression procedure.

The need to account for three time-dependent processes (see Appendix) demonstrates the influence of the corrosion reaction even at cathodic potentials. A common set of model parameters for each environment over the potential range studied could be successfully estimated only by including a time-dependent corrosion reaction in the model. Without the transient corrosion current, the time-dependent polarization curves would exhibit a static anodic current, which is inconsistent with collected anodic data.

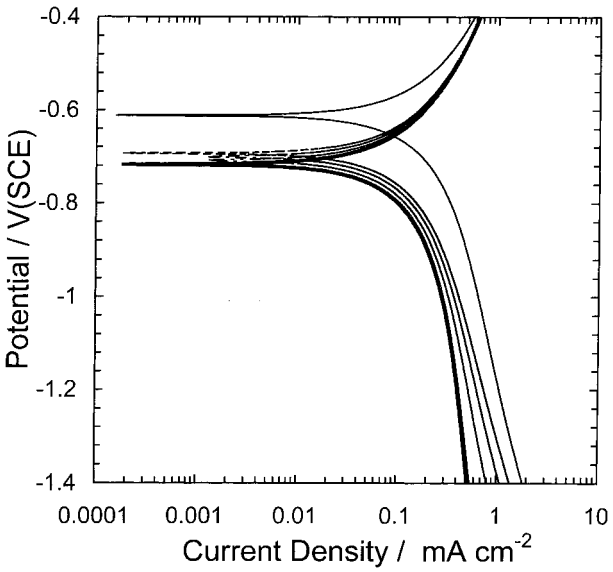

Fig. 5. Current–potential curves with reaction time as a parameter for the aerated HCHM electrolyte system. Curves do not change after two days. Key: (——) 0 h, (— — —) 2 h, (— — — —) 5 h, (— — — —) 10 h, (▬ ▬) 30 h, (▬ ▬) 50 h and (▬▬) 10 days.

5.3. *Identification of current contributions*

The structure of the physical model allowed for direct deconvolution of the time–dependent current–potential behaviour of the individual contributing reactions. The

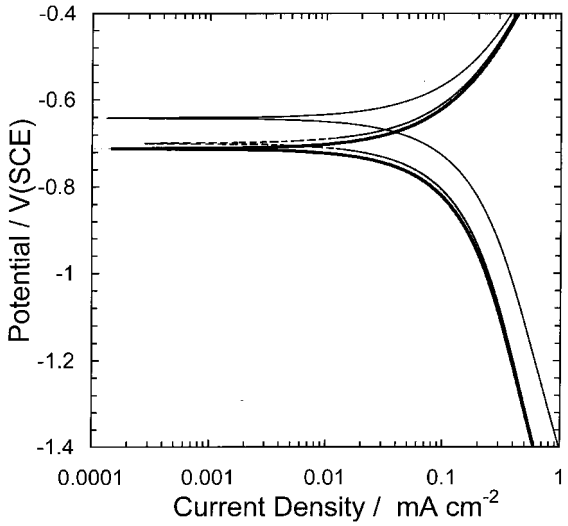

Fig. 6. Current–potential curves with reaction time as a parameter for the deaerated HCHM electrolyte system. Curves do not change after 5 h. Key: as for Figure 5.

Table 2. Parameters of the physical model for the system described in Section 3

Parameter	Aerated HCHM	Deaerated HCHM	Aerated HCLM	Deaerated *HCLM*
f_{∞,O_2}	0.701 ± 0.047	0.622 ± 0.190	0.521 ± 0.026	0.870 ± 0.026
τ_{O_2}/day	0.008 42 ± 0.000 71	0.068 80 ± 0.009 03	0.010 30 ± 0.000 55	0.209 ± 0.061
$i^*_{O_2}$/A cm^{-2}	7.56×10^{-4} ± 5.0×10^{-5}	2.34×10^{-4} ± 1.2×10^{-4}	5.47×10^{-4} ± 2.9×10^{-5}	2.07×10^{-4} ± 3.7×10^{-5}
f_{∞,H_2}	0.0685 ± 0.137	0.252 ± 0.159	0.174 ± 0.028	0.200 ± 0.070
$E^*_{H_2}$/V vs SCE	−2.866 ± 0.643	−2.813 ± 0.817	−2.391 ± 0.103	−2.993 ± 0.73
β_{H_2}/mV dec^{-1}	501.4 ± 124.0	579.8 ± 208.8	412.2 ± 255	601.0 ± 188.5
τ_{H_2}/day	0.311 ± 0.026	0.002 00 ± 0.000 32	0.422 ± 0.015	0.0105 ± 0.0011
$f_{\infty,Fe}$	0.882 ± 0.053	0.869 ± 0.084	0.7164 ± 0.0303	0.862 ± 0.055
E^*_{Fe}/V vs SCE	2.257 ± 0.155	2.581 ± 0.522	2.425 ± 0.072	2.530 ± 0.280
β_{Fe}/mV dec^{-1}	924.5 ± 49.6	953.4 ± 136.4	936.2 ± 24.6	896.7 ± 77.7
τ_{Fe}/day	0.004 77 ± 0.0011	0.033 80 ± 0.004 45	0.007 28 ± 7.2×10^{-4}	0.003 36 ± 21.98

current–potential curves for the corrosion, oxygen reduction and hydrogen evolution reactions are plotted in Figure 7 for the initial electrode conditions, the condition at 2 h, and the condition at 10 days for the steel electrode in the aerated HCHM environment. The change in the rate of each contributing reaction over time to the total current–potential curves for the deaerated HCHM system is shown in Figure 8. The oxygen reduction currents and the corrosion currents decrease to their final value in under two hours (for each reaction, the two hour and 10 day curves are superimposed). The hydrogen evolution current decreased more slowly than the other two currents.

As an example of the reduction in current required to maintain a constant applied potential, the process model predicts that a current density of approximately −3.44 A m^{-2} (−320 mA ft^{-2}) would be required initially to maintain an applied potential of −800 mV vs SCE. Over 10 days, Figure 7 illustrates that the corrosion current falls by 15%, the oxygen reduction current decreases by 50%, and the hydrogen evolution current diminishes by over 90%. Figure 6 shows that the overall reduction in current requirement at −800 mV vs SCE is 70%. The reduction over ten days in the contributing currents was less significant for steel in calcium-poor and magnesium-poor environments.

The generated time-dependent current–potential curves for API5LX52 pipeline steel in the aerated and deaerated HCLM environments are shown in Figures 9 and 10, respectively. The current–potential curves for

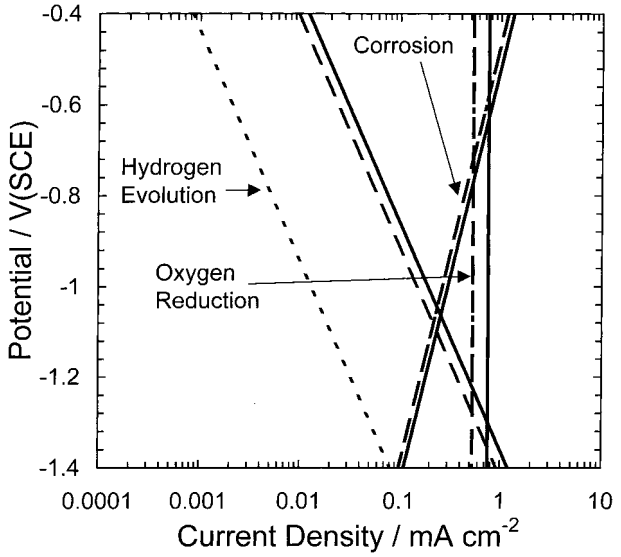

Fig. 7. Individual current-potential curves for the three contributing reactions (corrosion, oxygen reduction and hydrogen evolution) with time as a parameter for the aerated HCHM electrolyte system. Oxygen reduction and corrosion contributions do not change after 2 h. Key: (——) initial, (— —) 2 h and (– – – –) 10 days.

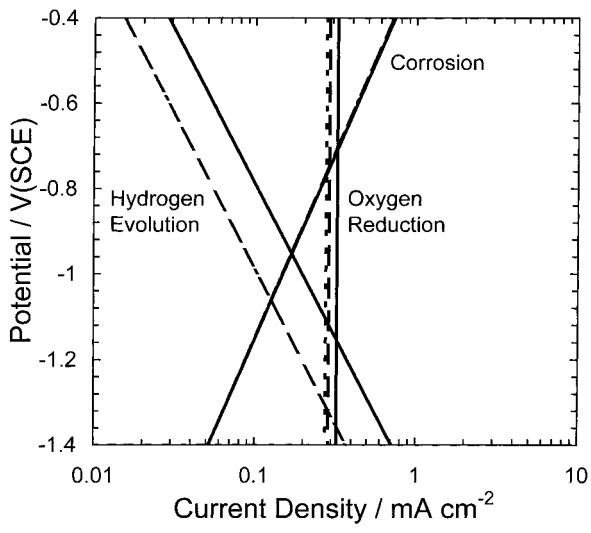

Fig. 8. Individual current–potential curves for the three contributing reactions (corrosion, oxygen reduction and hydrogen evolution) with time as a parameter for the deaerated HCHM electrolyte system. Corrosion contribution does not change significantly over 10 days. Hydrogen evolution current changes more dramatically than oxygen reduction current. Key: as for Figure 7.

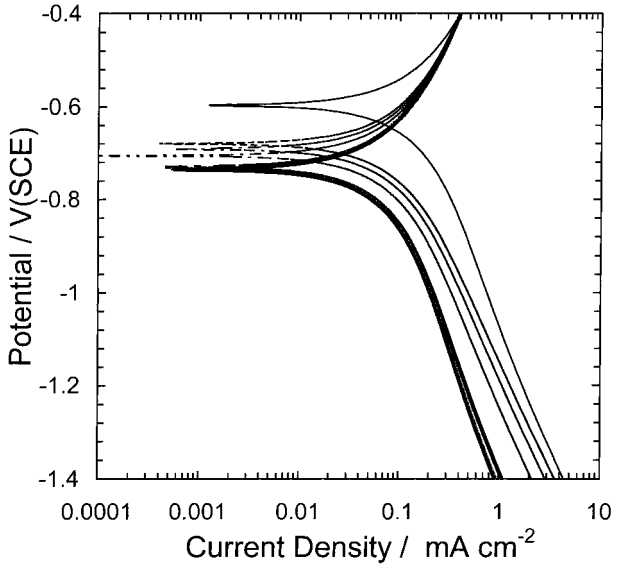

Fig. 9. Current–potential curves with reaction time as a parameter for the aerated HCLM electrolyte system. Curves do not change after two days. Key: (——) 0 h, (— — —) 2 h, (— — — —) 5 h, (— — — —) 10 h, (▬ ▬) 30 h, (▬ ▬) 50 h and (▬) 10 days.

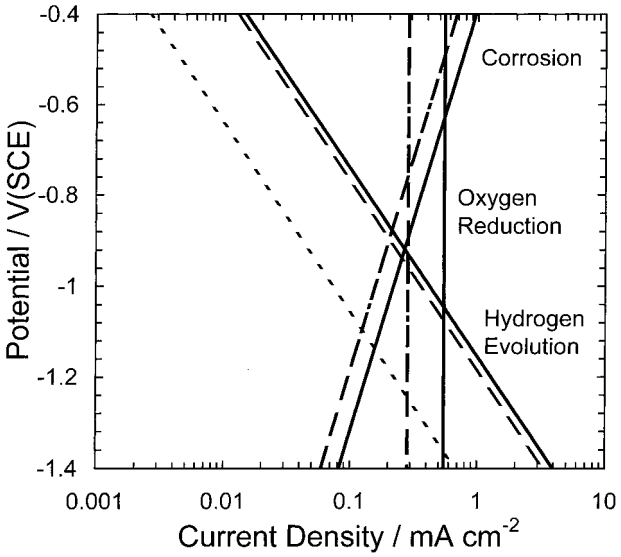

Fig. 11. Individual current–potential curves for the three contributing reactions (corrosion, oxygen reduction and hydrogen evolution) with time as a parameter for the aerated HCLM electrolyte system. Oxygen reduction and corrosion contributions do not change after 2 h. Key: (——) initial, (— —) 2 h and (▬ ▬) 10 days.

the corrosion, oxygen reduction, and hydrogen evolution reactions are plotted in Figure 11 (aerated HCLM) and Figure 12 (deaerated HCLM) for the initial electrode conditions, the condition at 2 h, and the condition at 10 days for the steel electrode in the aerated HCLM environment. The behaviour of the three reactions is similar for the HCHM and HCLM electrolyte systems.

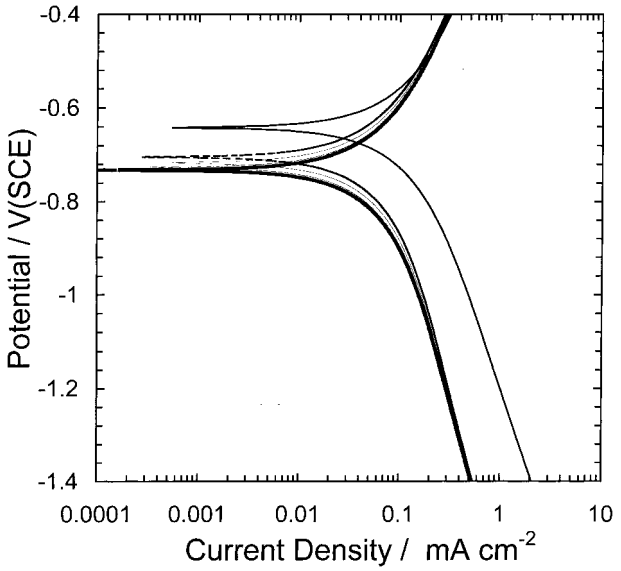

Fig. 10. Current–potential curves with reaction time as a parameter for the deaerated HCLM electrolyte system. Curves do not change after 10 h. Key: as for Figure 9.

Under aeration, the oxygen reduction currents and the corrosion currents decrease to their final value in under 2 h (for each reaction, the two hour and 10 day curves are superimposed). The hydrogen evolution current decreases more slowly than the other two currents. Under an argon atmosphere, the hydrogen evolution

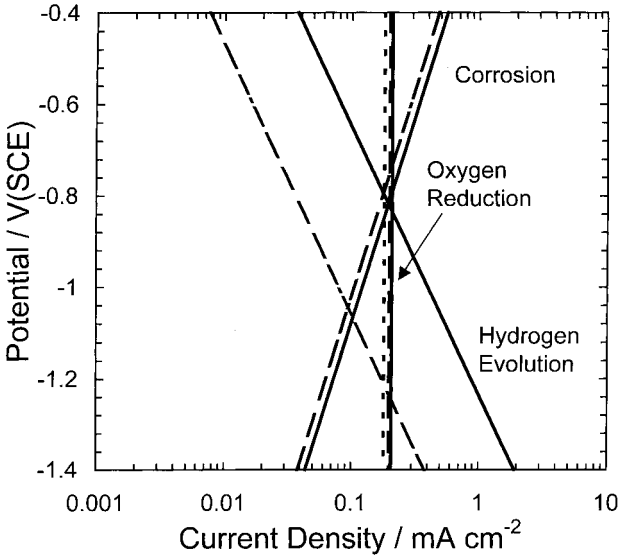

Fig. 12. Individual current–potential curves for the three contributing reactions (corrosion, oxygen reduction and hydrogen evolution) with time as a parameter for the deaerated HCLM electrolyte system. Corrosion contribution does not change significantly over 10 days. Hydrogen evolution current changes more dramatically than oxygen reduction current. Key: as for Figure 11.

reaction decays more rapidly and to a greater extent than the oxygen reduction reaction. The deconvolution of the model results suggests that the aeration level of the electrolyte is more important to the changes in reaction rates than is the concentration of calcareous ions.

Comparison between the curves predicted for the aerated and deaerated HCLM electrolyte system (Figures 9 and 10) suggests that the potential drop at open circuit are nearly equal. However, the shape of the curves in the two cases is quite dissimilar. Predictions for the aerated case show definite inflection points at very cathodic potentials which is consistent with the hydrogen evolution reaction becoming the dominant reaction in the system. The predicted curves for the deaerated case do not exhibit any such inflection point resulting from the lack of oxygen in the system. Thus, the model, in each case, behaves in a way which is consistent with the electrochemistry of the system.

5.4. *Model parameters*

Although a larger sample of electrolyte compositions should be used to confirm the results obtained here, a

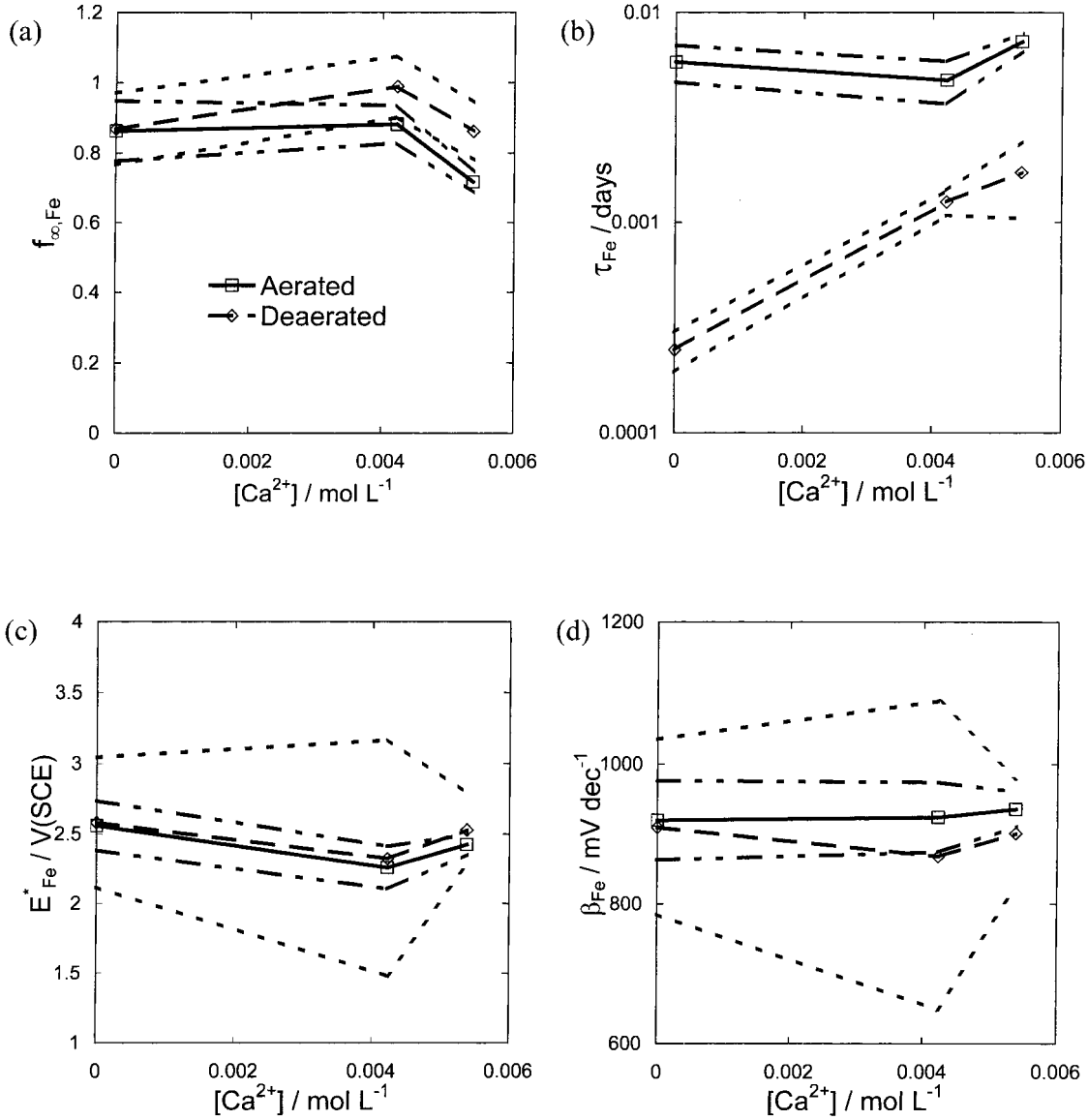

Fig. 13. Model parameters of the corrosion current as a function of calcium concentration. Connected points are of the same aeration content electrolytes. (a) Steady state contributing current fraction; (b) time constant; (c) reference potential; (d) Tafel slope. Key: (—□—) aerated and (—◇—) deaerated.

preliminary interpretation of the influence of aeration and ionic content on the regressed parameter values can be made.

5.4.1. *Corrosion*

The values of the parameters associated with the corrosion reaction are plotted in Figure 13 against the calcium content of the various electrolytes tested. The dashed lines represent the confidence interval obtained by regression. The steady state contributing current fraction parameter $f_{\infty,\mathrm{Fe}}$ was found to be independent of dissolved oxygen level or calcium content. This finding is consistent with the assumption made by Nisancioglu, et al. [4–6, 15] that the cathodic reactions do not affect the rate of corrosion of steel. The time constant τ_{Fe} associated with the corrosion reaction was affected by dissolved oxygen content, suggesting that the corrosion reaction reaches its steady rate more slowly in deaerated electrolytes than in aerated environments. The two kinetic parameters, E^*_{Fe} and β_{Fe}, were independent of dissolved oxygen content or calcium concentration. The independence of the two parameters with respect to aeration and calcium content is consistent with the assumption that E^*_{Fe} and β_{Fe} are independent of time.

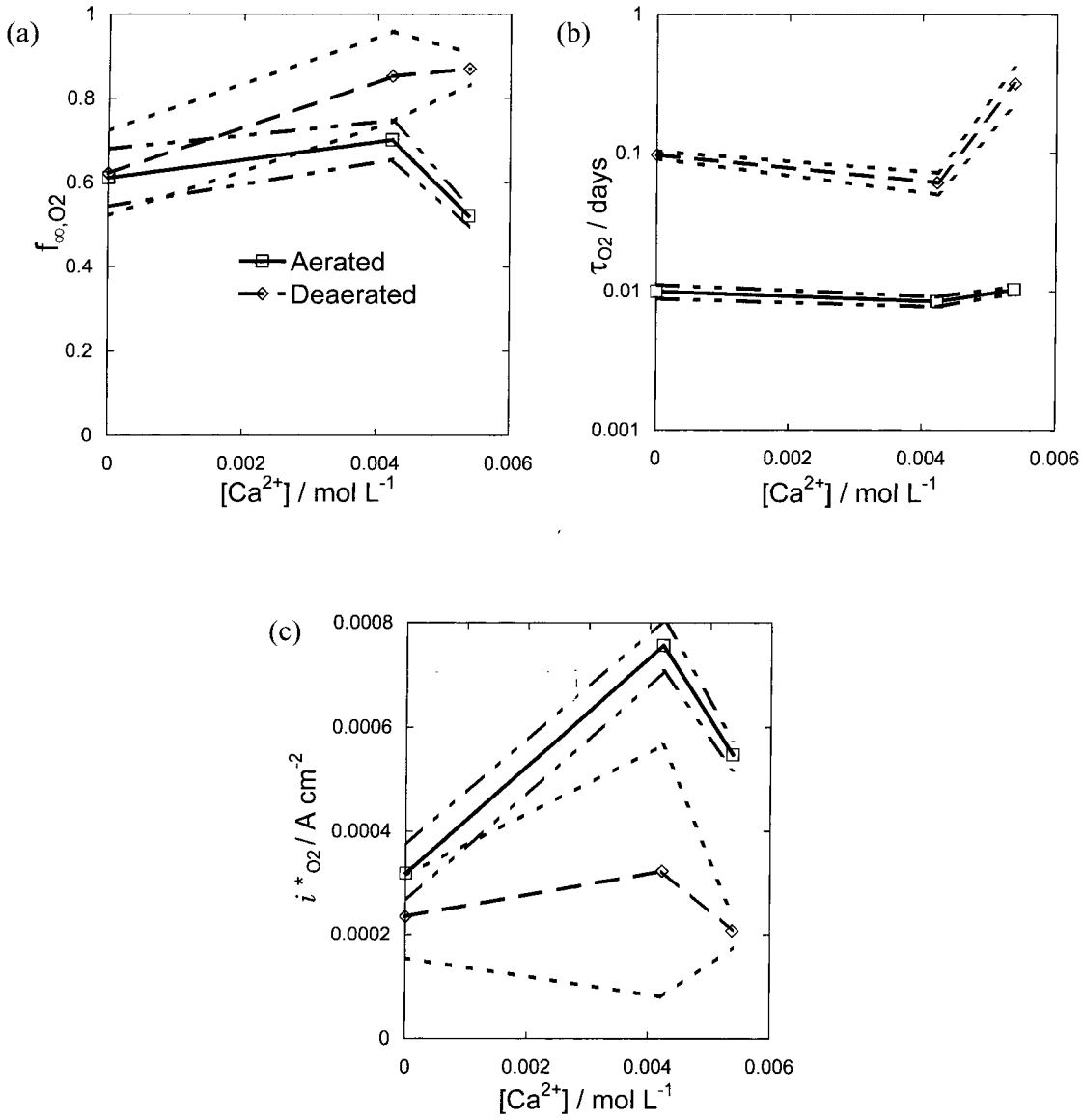

Fig. 14. Model parameters of oxygen reduction current as a function of calcium concentration. Connected points are of the same aeration content electrolytes. (a) Steady state contributing current fraction; (b) time constant; (c) mass transfer-limited oxygen reduction current. Key: (—□—) aerated and (—◇—) deaerated.

5.4.2. *Oxygen reduction*

Many of the parameters associated with the reduction of oxygen were dependent on aeration level (Figure 14). More data are needed to determine the dependence of f_{∞,O_2} on the dissolved oxygen content or on calcium concentration. The dependence of f_{∞,O_2} on electrolyte composition is an important issue. If the parameter is constant for all dissolved oxygen and calcium concentrations, the same level of protection should eventually be obtained for any calcium content or aeration level. The time constants associated with the reduction of oxygen, τ_{O_2}, and the mass transfer-limited oxygen reduction current, $i^*_{O_2}$, were clearly dependent upon dissolved oxygen content. The time constant was larger for the reaction in deaerated electrolytes; therefore, the barrier to the transport of oxygen was formed more rapidly in deaerated environments than in aerated electrolytes. The mass transfer-limited oxygen reduction current was generally larger in aerated electrolytes.

5.4.3. *Hydrogen evolution*

The parameters associated with the hydrogen evolution reaction are presented in Figure 15. The steady state contributing current fraction $f_{\infty_{H_2}}$ showed no distinct

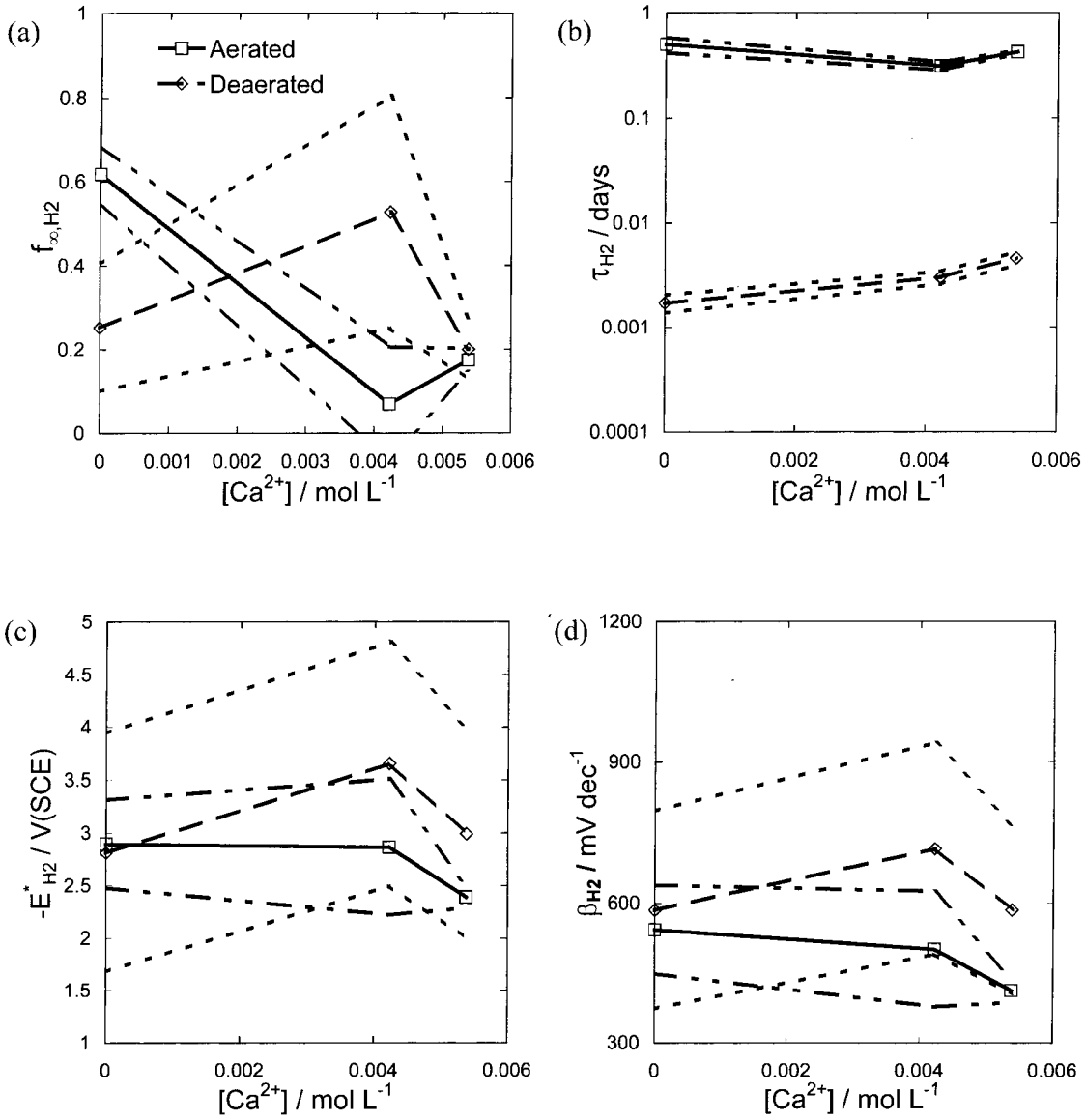

Fig. 15. Model parameters of the hydrogen evolution current as a function of calcium concentration. Connected points are of the same aeration content electrolytes. (a) Steady state contributing current fraction; (b) time constant; (c) reference potential; (d) Tafel slope. Key: (—□—) aerated and (—◇—) deaerated.

trending with aeration level or calcium concentration. The time constant for the reaction τ_{H_2} was strongly dependent on dissolved oxygen content. The hydrogen evolution reaction achieved a steady state more rapidly in aerated environments than in deaerated environments. The two kinetic parameters, $E^*_{H_2}$ and β_{H_2}, were independent of the dissolved oxygen and calcium concentrations. The small time constants for oxygen reduction and hydrogen evolution obtained in the present work are consistent with recent results obtained for synthetic and natural seawater [18, 20].

The results of these regressions are consistent with the values of $-0.1\,\mathrm{mA\,cm^{-2}}$ reported by Han [16] for the mass transfer-limited oxygen reduction currents in saturated HCLM and HCHM environments. The mass transfer-limited oxygen reduction current and the hydrogen evolution potential driving force would be of smaller magnitudes in drier soils [16].

Literature values for the Tafel slopes and equilibrium potentials for the hydrogen evolution and corrosion reactions are probably inappropriate for surfaces covered by calcareous films. The values obtained in this work for hydrogen evolution, for example, are on the order of 400 mV (decade)$^{-1}$ as opposed to the value of 174 mV (decade)$^{-1}$ assumed by Nisancioglu et al. [4–6, 15] Perhaps the most compelling argument in favour of the method used in this work is that the resulting parameters were found to be constants for a given environment. A common set of parameter values was found to apply for all measurements made at a given electrolyte composition and oxygen content. The success of the model is evident in that a fit to within less than 20 mV was obtained with parameters that were not functions of time or potential.

5.5. *Application to CP criteria*

The large Tafel slopes obtained in this work for the corrosion reaction imply that large shifts in potential are needed to reduce the corrosion current to a smaller value. For example, the value of Tafel slope reported in Table 2 means that a 924 mV shift is required to reduce the corrosion current by an order of magnitude. The magnitude of the Tafel slope, which is much larger than the 60 mV value expected for bare steel, can be attributed in part to the potential dependence of the calcareous deposits. The polarization requirements described here for a saturated soil matrix are much more severe than those reported for damp soils [16]. The experimental technique and associated regression procedure could be employed for soils of controlled moisture content to obtain values more representative of field applications.

6. Conclusions

The experimental system described provided bench-top measurements of the current–potential–time response of pipeline steel to formation of deposits in electrolytes designed to simulate soil leachate compositions. The system was designed to provide uniform current and potential distributions over the electrodes; thus the analysis did not require correction for nonuniform reaction kinetics. All experiments were performed in an inert solid matrix (silicate sand). Replenishment of electrolyte was required to avoid pitting on the steel surface.

The time constants for the influence of the growth of calcareous deposits and corrosion products influence the overall current response at cathodic potentials near the corrosion potential. The three-time constant process model used to describe the results provided a common set of parameters for a given soil environment and level of aeration. The parameters estimated were valid for all applied current values and were independent of time, potential and applied current.

The experimental approach and regression procedure model used are general and could be used to determine the physical parameters associated with the seasonal variations (wet–dry cycles) in the soils surrounding pipelines or with other factors that influence general corrosion. The polarization model provides critical information that could be used as a boundary condition in mathematical models for cathodic protection of pipelines or other buried structures. The separation of current contributions implicit in the model can be used to assess the reduction of corrosion current associated with specific CP criteria.

Acknowledgements

This work was supported by PRC International via Contract RPTG/PR: 101–9221. A full report of [21] is available from the American Gas Association. The authors thank the Corrosion Supervisory Committee of PRC International for their oversight and suggestions.

Appendix: Time-domain measurement model

The frequency domain measurement model approach developed for spectroscopy measurements [24–31] was extended to provide a time-domain measurement model to extract the number of independent time-dependent processes represented in a potential–time trace. The

model accounted for processes leading to exponentially decaying increases or decreases in potential, that is,

$$V - \Phi_{\text{ref}} = a_0 + \sum_{m=1}^{j} a_m \exp(-t/\tau_m) + \sum_{n=1}^{k} b_n(1 - \exp(-t/\tau_n)) \quad (17)$$

where $a_0 + \sum_{n=1}^{k} b_n$ represents the potential obtained as time approaches infinity. The model was regressed to individual potential–time traces using the Marquardt–Levenberg method [23]. The requirement that the confidence interval for parameter estimates not exceed their 95.4% confidence interval was used to identify the maximum number of exponential lineshapes.

Data taken from preliminary experiments in which the electrolyte was not replenished revealed an exponential decay followed by an exponential increase in potential. Visual inspection of the coupons after the experiment revealed corrosion by pitting. Once fresh electrolyte was fed continuously, pitting was no longer observed, and a time increasing function could no longer be regressed to the measured potential–time traces. With the exception of the most anodic and cathodic currents, three exponential decay lineshapes could be identified by the regression procedure. At very anodic currents, the hydrogen evolution reaction is expected to provide a negligible contribution to the total current. Likewise, the corrosion reaction current is expected to be insignificant at very cathodic currents. The time decay processes were taken to be associated with the effect that the formation of films would have on the three contributing reactions. No lineshape associated with an increase in potential could be resolved from the data after the system was modified to refresh the electrolyte.

References

1. A.W. Peabody, 'Control of Pipeline Corrosion', NACE Publications, Houston, TX (1967).
2. J. Morgan, 'Cathodic protection', 2nd edn (NACE Publications, Houston, TX 1993).
3. R.U. Lee and J.R. Ambrose, *Corrosion* **44** (1988) 887–891.
4. K. Nisancioglu, *Corrosion* **43** (1987) 100–111.
5. K. Nisancioglu, P.O. Gartland., T. Dahl and E. Sander, *Corrosion* **43** (1987) 710–18.
6. K. Nisancioglu and P.O. Gartland, 'Current Distribution With Dynamic Boundary Conditions', *I. Chem. symposium Series No. 112: Conference on Electrochemical Engineering*, Loughborough University of Technology, Loughborough UK (April, 1989).
7. S.N.R. Yan, Pakalapati, T.V. Nguyen, R.E. White and R.B. Griffin, *J. Electrochem. Soc.* **139** (1992) 1932–6.
8. K.J. Kennelley, L. Bone and M.E. Orazem, **49** (3) (1993) 199–210.
9. S.N.R. Yan, Pakalapati, T.V. Nguyen, R.E. White and R.B. Griffin, *J. Electrochem. Soc.* **139** (1992) 1932–6.
10. M.E. Orazem, L. Bone and K.J. Kennelley, *Corrosion* **49** (1993), 211–9.
11. R.M. Degerstedt, K.J. Kennelley, M.E. Orazem and J.M. Esteban, *Mater. Perform.* **35** (1996) 16–20.
12. M.E. Orazem, J.M. Esteban, K.J. Kennelley and R.M. Degerstedt, *Corrosion* **53** (1997) 264–72.
13. M.E. Orazem, J.M. Esteban, K.J. Kennelley and R.M. Degerstedt, *Corrosion* **53** (1997) in press.
14. W.H. Hartt, C.H. Culberson and S.W. Smith, *Corrosion* **40** (1984) 609–18.
15. K. Nisancioglu, *in* 'Modern Aspects of Electrochemistry' Vol. 23 (edited by R. White, J. O'M Bockris and B. E. Conway, (Plenum Press, New York, 1992), p 149.
16. M.K. Han, 'Effects of Seasonal Variations on Requirements to Prevent Corrosion in Soils', Final Report PR-3-505 to the Corrosion Supervisory Committee of the American Gas Association (Dec. 1988).
17. J. J. Morgan and W. Stumm, 'Aquatic Chemistry: An Introduction Emphasizing Chemical Equilibria in Natural Waters' (John Wiley & Sons, New York, 1981).
18. O. Gil, S. Touzain, C. Deslouis, B. Tribollet, C. Compere and D. Feisty, 'In situ characterization of calcareous layers formed in synthetic sea water', presented at the 3rd International Symposium on Electrochemical Impedance Spectroscopy, 7–12 May (1995), Nieuwpoort, Belgium.
19. J.S. Luo, R.U. Lee, T.Y. Chen, W.H. Hartt and S.W. Smith, *Corrosion* **47** (3) (1991) 189–196.
20. C. Deslouis, A. Doncescu, D. Feisty, O. Gil, V. Maillot, S. Touzain and B. Tribollet, 'Kinetics and characterization of calcareous deposits under cathodic protection in natural seawater', presented at the 6th International Symposium on Electrochemical Methods in Corrosion Research, 25–29 Aug. (1997), Trento, Italy.
21. M.E. Orazem and S.L. Carson, 'Time-Dependent Polarization behaviour as a Function of Soil Type', Catalogue L51735, PRC International at the American Gas Association, Arlington, VA (1995).
22. J. Newman, *J. Electrochem. Soc.* **138** (1991) 3554–60.
23. W. H. Press, B. P. Flannery, S. A. Teukolsky and W. T. Vetterling, 'Numerical Recipes: The Art of Scientific Computing (FORTRAN Version)' (Cambridge University Press, 1989).
24. P. Agarwal, M. E. Orazem and LH. García-Rubio, *J. Electrochem. Soc.* **139** (1992) 1917–27.
25. P. Agarwal, O. C. Moghissi, M. E. Orazem and L.H. García-Rubio, *Corrosion*, **49** (1993) 278–89.
26. M. Orazem, P. Agarwal, A.N. Jansen, P.T. Wojcik and L.H. García-Rubio, *Electrochem. Acta* **38** (1993) 1903–11.
27. P. Agarwal, Oscar D. Crisalle, M. E. Orazem and L.H. Garrcía-Rubio, *J. Electrochem. Soc.* **142** (1995) 4149–58.
28. P. Agarwal, M.E. Orazem and L.H. García-Rubio, *J. Electrochem. Soc.* **142** (1995) 4159–68.
29. M.E. Orazem, P. Agarwal and L.H. García-Rubio, *Mater. Sci. Forum* **192–194** (1995) 563–72.
30. M.E. Orazem, P. Agarwal, C. Deslouis and B. Tribollet, *J. Electrochem. Soc.* **143** (1996) 948–60.
31. M.E. Orazem, T. El Moustafid, C. Deslouis and B. Tribollet, *J. Electrochem. Soc.* **143** (1996) 3880–90.